Broadband Near-Unidirectional Absorption Enabled by Phonon-Polariton Resonances in SiC Micropyramid Arrays

G. C. R. Devarapu[1,2,3] and S. Foteinopoulou[1,4,*]

[1]School of Physics, College of Engineering, Mathematics and Physical Sciences (CEMPS), University of Exeter, Exeter EX4 4QL, United Kingdom
[2]School of Physics and Astronomy, University of St. Andrews, North Haugh, St. Andrews KY16 9SS, United Kingdom
[3]Cork Institute of Technology, Bishoptwon, Cork T12 P928, Ireland
[4]Center for High Technology Materials, University of New Mexico, 1313 Goddard Street SE, Albuquerque, New Mexico 87106, USA

(Received 23 November 2016; published 3 March 2017)

Inspired by moth eyes, nature's most powerful antireflex, we present a subwavelength SiC micropyramid design, which operates in the reststrahlen band of SiC, namely, the spectral band of strong phonon-photon coupling in the SiC material. While within this band, SiC repels electromagnetic waves, we observe here a broad low-reflectivity window with unique attributes, with distinct characteristics different from typical dielectric moth-eye-like structures. To be specific, while the latter systems are entirely symmetric, the reflection response of our SiC micropyramid system can be highly asymmetric. In particular, the SiC micropyramid system can be near reflectionless for light impinging from the tip side of the micropyramids and can exhibit more than 90% reflection for light impinging from the base side of the micropyramids, over a broad wavelength range in the SiC reststrahlen band. This strongly asymmetric reflection response emanates from the cascaded coupling of vortexlike cavity modes at each of the SiC blocks comprising the micropyramids and translates into a strongly unidirectional absorber response. We discuss how, by virtue of Kirchhoff's law, this strongly unidirectional superabsorber behavior implies a strongly unidirectional emission profile that is important for one-way infrared sources and passive-radiative-cooling systems.

DOI: 10.1103/PhysRevApplied.7.034001

I. INTRODUCTION

Across the electromagnetic (EM) spectrum, recent intense research efforts aim to uncover new mechanisms for extreme absorption control that go beyond the traditional three-component platforms with the absorber sandwiched between an antireflex coating and a back reflector. The driving forces behind these investigations are photovoltaic devices [1–4] as well as infrared and terahertz detectors [5–9], modulators [9,10], and thermal emitters [7,9,11,12]. The strategies underpinning these current absorption management efforts can be grouped into five general approaches. In particular, new superabsorber architectures that have been proposed may utilize plasmonic resonances that enhance the EM field in the vicinity of the absorber [1,3,13], involve photonic metamaterials [14,15] either as impedance matchers [5,16,17] or enhancers of dark EM-field components by virtue of a characteristic hyperbolic photonic dispersion [18], employ lossy material bilayers with destructive Fabry-Perot interference-suppressing reflection [9,19], tailor resonant coupling to waveguide or cavity modes in the absorber structure [4,12], or manipulate a near-reflectionless coupling to the near-band-edge Floquet-Bloch mode of a lossy photonic crystal [20,21].

Of the aforementioned avenues to extraordinary absorption management, the last two are particularly attractive, as they essentially represent one-step superabsorber platforms. That is to say, the functional performance of these structures relies only on a single kind of absorbing medium; it is not needed to incorporate another type of metallic or absorber material that may make fabrication more complicated, lead to parasitic absorption [3,5], or compromise structural stability due to overheating. This is not the case for any of the other schemes, where together with the absorber of interest, additional patterned absorber or metallic material are integrated to enable impedance matching [5,19,22], EM-field enhancement [1,3], or additional light passes [22,23].

Now, the valuable insight obtained for absorption with plasmonic nanostructures in the visible spectrum [2] can be transferred in the mid-IR spectral regime, albeit not with the use of metals. Metals in the infrared spectrum have a very small skin depth; thus, they repel the EM field and do not respond with the familiar plasmonic resonances existing in the visible spectrum. However, "plasmonic effects" in the mid-IR can be mimicked if we instead

*Corresponding author.
sfoteino@unm.edu

consider microstructures comprising material with a strong phonon-photon coupling. Such phonon-polariton materials can exhibit a negative permittivity response in the mid-IR with a larger skin depth. They so emulate field-confinement effects with infrared light similar to those of plasmonic nanostructures [24] operating in the visible spectrum.

Thus, for mid-IR absorption platforms, SiC is an excellent material with its phonon-polariton gap spectrum (reststrahlen band) between 10.3 to 12.6 μm [25]. This spectral regime is of high interest for detectors and sources, as it encompasses the absorption fingerprints of many biomolecules [26]. Moreover, this spectrum is also highly relevant to passive-radiative-cooling devices [27], since it lies within the atmospheric transparency window [28,29]. In addition, SiC is a refractory material, which is crucially important for the structural stability of absorber or emitter devices [30].

In this paper, we investigate SiC-based designs with the objective to achieve mid-IR subwavelength broadband superabsorption [2,31–33] that is also highly unidirectional. Designing and controlling a highly unidirectional mid-IR absorption response has not been thus-far investigated but can benefit various applications. In particular, highly unidirectional absorbers efficiently absorb light that impinges from their top side while they reflect and, thus, not absorb, almost all light that impinges from their bottom side. Kirchhoff's law then prescribes [34,35] that these systems emit light predominantly towards the direction where they are strong absorbers if light is incident from that direction, in this manner acting as near-unidirectional emitters. Unidirectional emission is a highly attractive feature not only for the design of one-way infrared sources but also for simpler integrated components for passive-radiative-cooling devices to reduce temperature in buildings [27] or electronic circuits. In order to achieve this goal, we bring together two of the aforementioned explored avenues for harnessing absorption, i.e., invoking cavity resonances and photonic crystal (PC) effects and combine them with intuition obtained from the antireflex properties of moth-eye-like structures. This allows us to consider SiC-only platforms without other auxiliary absorbing material structures that can compromise the resilience of the device under high temperatures.

This paper is organized as follows: In Sec. II, we present the SiC-based platform we envision for strong absorption control within the reststrahlen band of SiC. In Sec. III, we present our results for an initial design demonstrating enhanced broadband absorption. We discuss the origin of such absorption enhancement with respect to bulk SiC in the same frequency region in Sec. IV. In Sec. V, we analyze the effects of a stronger interaction between the micropyramid building blocks towards a broadband superabsorber [2,31–33] behavior. In Sec. VI, we quantify the absorption enhancement and demonstrate the robustness under misalignment of the micropyramid superabsorber platform. In Sec. VII, we investigate the asymmetric absorber response for light illuminating from the tip side and base side of the micropyramid-array platform. In Sec. VIII, we discuss how this asymmetry can be harnessed further towards a near-unidirectional absorber or emitter behavior. Finally, in Sec. IX, we present our conclusion.

II. THE SILICON CARBIDE PLATFORM FOR BROADBAND SUPERABSORPTION

In spite of silicon carbide's high loss tangent within its reststrahlen band, which makes it potentially attractive for absorber or emitter systems, it is actually extremely difficult to couple light inside the SiC material in this spectrum; most light gets reflected upon hitting the SiC surface. This low in-coupling poses a serious bottleneck in SiC-based absorber or emitter platforms. However, recent results with a compact one-dimensional SiC judicious PC design [21] show that it is possible to suppress such reflection and achieve near-perfect absorption within a narrow spectral band. This band can be extended to cover most of the SiC reststrahlen spectral region by employing a very thick, several-wavelengths-long PC [36]. However, in practical applications, it is desirable to have compact designs exhibiting a broadband superabsorption [31–33]. In addition, we seek such superabsorber merit to be highly asymmetric, i.e., to exist only for light impinging from one side of the structure.

In order to achieve our target of a broadband absorption in SiC within its reststrahlen band with a compact structure, we employ a design with a SiC micropyramid as its elementary building block arranged in a one-dimensional photonic crystal array. We draw our inspiration for such a design from the conical shape of corneal nipples in moth eyes [37,38], which are known for their superior antireflection properties. The moth-eye corneal nipples do not constitute an optically dense material, so naturally, one may wonder whether designs of a similar shape but made from a material with extreme optical properties, such as SiC in the reststrahlen band, will retain these extraordinary antireflex properties. Antireflection behavior has been demonstrated [39,40] in the optical spectrum with nanostructured cones or pyramids mimicking moth eyes comprising a high-refractive-index material, such as GaP or Si, which have a purely dielectric optical response. These results provide a promising basis to expand such antireflex behavior in a platform made of SiC, whose material optical response in the reststrahlen band involves both a negative permittivity and an optical loss tangent (see bottom left inset in Fig. 1) due to the photon-phonon coupling resonance in this spectrum. Thus, we proceed with our intuitive choice of SiC-micropyramid-based designs, which we investigate further in the following.

We show the design under consideration in Fig. 1. We consider a stepped two-dimensional (2D) pyramid, with translational symmetry in the third dimension. The

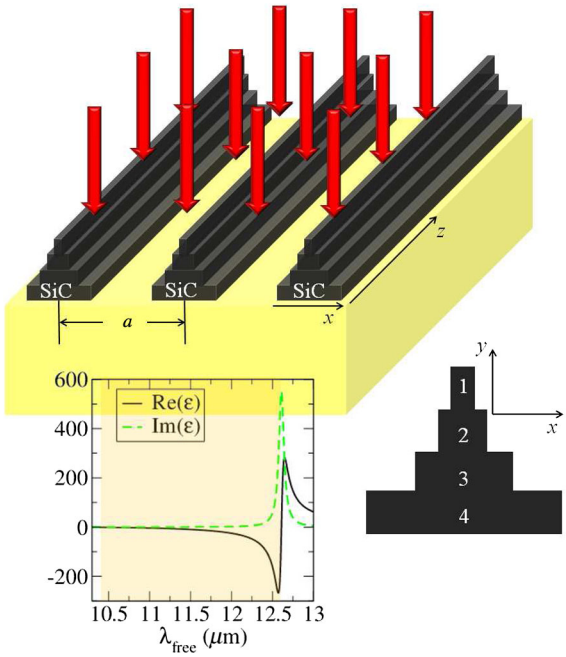

FIG. 1. The 2D SiC moth-eye superabsorber (the structure is assumed to be infinite in the z direction). The bottom right panel represents a front view of the SiC stepped micropyramid, where we designate with a numeral each participating block. We also show in the bottom left panel the permittivity ε of bulk SiC [real (black solid line) and imaginary (dashed green line) parts] in the reststrahlen band (yellow shaded region), where the strong photon-phonon coupling yields a negative permittivity.

translational symmetry ensures full polarization decoupling [41] allowing for polarization-selective emission suitable for constructing polarized infrared sources. Moreover, we consider a stepped micropyramid structure, whose realization is possible with certain fabrication techniques, such as direct wafer bonding [42] or layer-by-layer fabrication with e-beam patterning [43] and inductively-coupled-plasma reactive-ion etching [44].

Each block of the micropyramid is expected to behave as a resonant cavity [45] microantenna with emission or absorption spectra in the mid-IR regime. By combining blocks of different sizes, we aim to bring together different resonant frequencies, thus, constructing a broadband response for the pyramid microantenna. Then, by arranging the pyramid blocks in a moth-eye structure, we aim to minimize reflection, thus, enabling a strong EM incoupling to each of the participant block microresonators. That is to say, our proposed design is conceived with a vision to operate simultaneously as a moth-eye antireflector and a broadband microantenna.

The sizes of the participating SiC blocks in the pyramid of Fig. 1 are chosen so that a gradual size variation from one block to the next one is maintained, with a small number of layers, which is desirable from the fabrication point of view. At the same time, we aim for a compact structure of subwavelength total thickness, i.e., thickness in the order of half the free-space wavelength. In Fig. 1, we label each of the blocks comprising the micropyramid with 1, 2, 3, and 4. Their corresponding sizes (in the x and y directions, respectively) are $w_{x1} = 0.5\ \mu$m, $w_{y1} = 1\ \mu$m, $w_{x2} = 1\,\mu$m, $w_{y2} = 1\,\mu$m, $w_{x3} = 2\,\mu$m, $w_{y3} = 1\,\mu$m, $w_{x4} = 4\,\mu$m, and $w_{y4} = 1\ \mu$m.

These micropyramids are arranged periodically in an array with a spacing a. We vary this interspacing a so we can control the system's collective response from a regime where each micropyramid responds independently to the impinging light to a regime where the resonances between neighboring micropyramids are interacting. In our initial investigation, we ignore the presence of a required substrate seen in Fig. 1 in order to capture and understand the response of our proposed microstructure better. We then consider the effect of the substrate afterward. So, unless we explicitly state the presence of a substrate, all results correspond to the platform of Fig. 1 but without the depicted substrate.

III. ENHANCED ABSORPTION WITH THE SiC MICROPYRAMID SYSTEM

We first study the response of the micropyramid-array system, where each micropyramid building block responds independently to the impinging light. For this purpose, the micropyramids are placed sparsely, about one free-space wavelength apart, with an interspacing of $a = 10\ \mu$m. We consider normally incident light and both polarization cases, where the impinging light has its electric field aligned with the micropyramid block-axis z (TE polarization) or its magnetic field aligned with the micropyramid block-axis z (TH polarization). We use a two-dimensional implementation of the finite-difference time-domain (FDTD) method with the Lumerical FDTD simulator [46] to investigate the response of the micropyramid-array system.

In the FDTD simulator, periodic boundary conditions are applied in the x direction as the micropyramid building blocks repeat themselves periodically in this direction. Open (absorbing) boundary conditions are applied in the y direction to emulate an unbounded domain above and below the micropyramid. The micropyramid structure is discretized in the simulation with a mesh size of $dx = dy = 10$ nm. In our calculations, we consider a SiC permittivity function characteristic of the phonon-polariton resonant response in the reststrahlen band, i.e.,

$$\varepsilon(\omega) = \varepsilon_\infty \left(1 + \frac{\omega_L^2 - \omega_T^2}{\omega_T^2 - \omega^2 - i\omega\Gamma}\right). \tag{1}$$

The high-frequency response ε_∞, the longitudinal and transverse optical phonon frequencies ω_L and ω_T, respectively, and the intrinsic damping parameter Γ are determined by fitting to experimental optical data [25]. From

Ref. [25], we take $\varepsilon_\infty = 6.7$, $\omega_L = 2\pi \times 29.07$ THz, $\omega_T = 2\pi \times 23.79$ THz, and $\Gamma = 2\pi \times 0.1428$ THz. The SiC permittivity spectral function corresponding to Eq. (1) is depicted in the bottom left inset of Fig. 1.

We clearly observe in Fig. 2 that the micropyramid-array system responds very differently to TE and TH light. For TE light, the system shows both very little reflection and very little absorption [solid black lines of Figs. 2(a) and 2(b), respectively]. This is because the electric field drives the phonon-polariton resonance along the z direction where the SiC material is unbounded. Thus, the EM field behaves as in the vicinity of bulk SiC and penetrates the SiC micropyramid only very little. However, since the micropyramid array is arranged sparsely, the EM field can flow around the structure yielding a very low absorption and high transparency. Indeed, we confirm that as we bring the micropyramids closer, the reflective response of the micropyramid system to TE light becomes similar to that of bulk SiC. Clearly, the SiC micropyramid-array structure is a weak absorber or emitter for TE-polarized light.

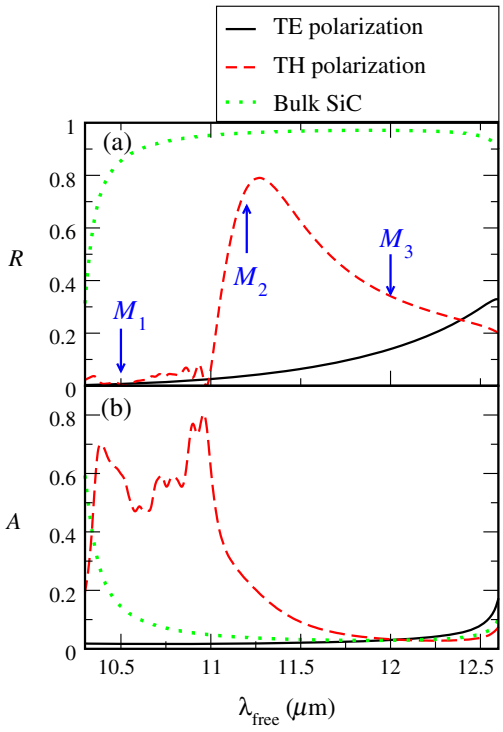

FIG. 2. Spectral response versus the free-space wavelength λ_{free} of the SiC micropyramid array under normal incidence for the TE (TH) polarization case [solid black (dashed red) lines]. In (a) [(b)] the reflectance R [absorptance A] is shown. In addition, the reflection (absorption) from bulk SiC is shown in (a) [(b)] for comparison with dotted green lines. We designate with M_1, M_2, and M_3 selected modes, each falling in one of the three characteristic spectral regimes: the broadband reflectionless region, the region near the reflection maximum, and the second low-reflectivity window past the occurrence of the reflection peak.

On the other hand, for TH-polarized light, we observe in Fig. 2 a wide low-reflectivity window within the SiC reststrahlen band between approximately 10.3 and 11.1 μm [dashed red line in Fig. 2(a)], in spite of bulk SiC being nearly perfectly reflecting in this range [dotted green line in Fig. 2(a)]. This low-reflectivity window translates into a broad absorption window with absorption exceeding 50% for the most part and reaching values as high as 80% [dashed red line in Fig. 2(b)]. This highly efficient absorption represents extraordinary absorption-enhancement factors, as high as 16, with respect to the absorption capabilities of bulk SiC [dotted green line in Fig. 2(b)]. We note that a second window that we observe with relatively low reflection appearing close to the red bound of the reststrahlen band is not accompanied by a high absorption. Clearly, we see in Fig. 2(b) that absorption is negligible within that range. We note in passing, that these two aforementioned spectral windows are separated by a spectrum with a high-reflection response. In this intermittent regime, reflection reaches a maximum of about 80% at an impinging wavelength of 11.27 μm, with an asymmetric peak that is typical of Fano resonances [47].

IV. UNDERSTANDING THE ABSORBER BEHAVIOR OF THE SiC MICROPYRAMID SYSTEM

Clearly, the results in Fig. 2 demonstrate that the design of Fig. 1 has strong potential as a superabsorber for TH-polarized light, which we explore further in the following. Therefore, we attempt to understand better the response of the micropyramid array by looking at the spectral response of each element it comprises. In other words, we look at the spectral response of a periodic array comprised only of the top block, the second block, the third block, and the fourth block of the micropyramid, respectively, as designated in the bottom panel of Fig. 1. We show these results for the reflection R and absorption A in Figs. 3(a) and 3(b), respectively, with a dotted red line (top block array), solid black line (second block array), dashed green line (third block array), and dot-dashed blue line (fourth block array). The arrays comprising either of the first two blocks have near-zero reflective properties. These block sizes are deep subwavelength, thus, only minimally disturb the path of the incident light. However, clear resonances still exist, as we observe by the peaks in the absorption spectrum and the enhanced electric field within the SiC block. For example, see the inset depicting the electric-field-intensity enhancement within the first block for the free-space wavelength $M1$.

The behavior is similar for the arrays comprised of either the third or fourth block, as we see from the peaks in the absorption spectrum and the electric field enhancement inside the blocks (for example, see the inset for the fourth block for the free-space wavelength $M1$). All blocks show a resonant response over a relatively broad spectrum, with

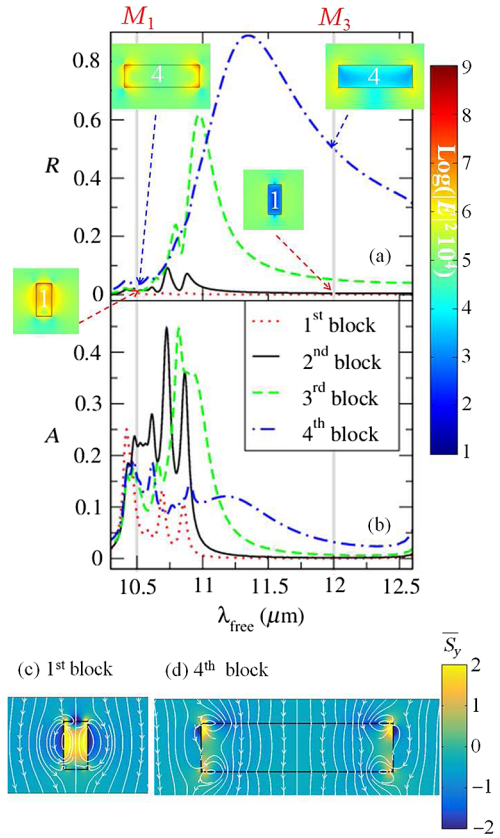

FIG. 3. Spectral reflection response (a) and absorption response (b) of the different periodic arrays made of the respective individual blocks comprising the pyramid of Fig. 1. The two characteristic frequencies or free-space wavelengths in the vicinity of the cavity and void resonances marked as $M1$ and $M3$, respectively, are designated with the gray vertical lines. The insets depict the electric field intensity around the SiC block [48] for the respective arrays comprising the first or fourth of the micropyramid's blocks for these two frequencies. Note, the corresponding color map on the top right of the figure is in logarithmic scale. In addition, we show in panels (c) and (d) the energy circulation (white streamlines with arrows) around the first and fourth blocks, respectively, for the frequency $M1$. Note, in (c) and (d) the background color map represents the y component of the time-averaged Poynting vector $\bar{S}_y$ [49]; hence, negative values represent a downward EM flow.

the larger blocks sustaining resonances through longer wavelengths. We observe in Fig. 3 that for the large blocks, the resonances are characterized by strong fields at the corners, while for the smaller block, the field is more uniform, with stronger fields at the sides of the block.

The resonances and their corresponding electric field morphology arise from the surface phonon polaritons at the facets of the SiC blocks and their interaction. Note that it is the strong phonon-photon coupling in SiC that yields a negative permittivity to SiC, thus, enabling surface bound modes similar to those of metals at optical frequencies [50]. As a result of such surface bound modes, resonant optical trapping occurs within the blocks, as one can observe from the EM-energy circulation plots (white streamlines) in Figs. 3(c) and 3(d) for the cases of the first and fourth blocks, respectively. We clearly identify vortices in the EM circulation in either the sides [case seen in Fig. 3(c)] or in the vicinity of the corners [case seen in Fig. 3(d)]. These vortices signify the existence of cavitylike optical trapping behavior [51]. On the other hand, for the lower frequencies near the red bound of the reststrahlen band, we do not find any block-cavity modes, as the field goes around the block (for example, see the insets in Fig. 3 for blocks 1 and 4 for frequency $M3$).

It is interesting to observe that the arrays comprising the third or fourth block individually demonstrate a clear asymmetric reflection peak, as we see in Fig. 3(a), which separates the spectral regime where localized resonant modes exist within the block—for example, as we see from the electric field inset for the fourth block at free-space wavelength $M1$ from the spectral regime where void modes are excited in the interstitial region between the neighboring blocks and as we see, for example, from the electric field inset for the fourth block at free-space wavelength $M3$. In these void modes, the electric field is near zero within the block.

It is the former spectral regime, i.e., the regime of block-cavity resonances, that is evidently of interest with respect to achieving superabsorption. This is because in order to harness a strong absorption response, the strong electric fields must spatially overlap with the absorbing matter. This follows directly from Poynting's theorem for power dissipation [see, also, Eq. (A3)]. In passing, we also note that the presence of the spectrally asymmetric reflection peak observed in Fig. 3 suggests the occurrence of a Fano-type interference [47] at that frequency that arises from the interference between the localized resonant block modes that are present at the shorter-wavelength side of the reststrahlen band and the extended nonresonant [52] void modes that are present at the longer-wavelength side of the reststrahlen band. However, the spectral region we focus on here is the frequency regime near the blue bound of the reststrahlen band. This is the frequency regime where the localized block-cavity modes are excited, yielding the strong electric field required to achieve a strong absorption. In other words, the SiC blocks behave as microantennas in this spectral region.

Now, let us compare the spectral reflection response of the entire pyramid array with that of the individual-block arrays. We observe that the micropyramid array has a hybrid response borrowing characteristics from the reflection response of the different individual-block arrays. In particular, the reflection response of the micropyramid array for the spectral regions of the Fano interference and void resonances is dominated by the reflection response of the largest constituent block. On the other hand, the respective reflection response for the spectral region where the localized cavity modes are excited mimics

the near-zero reflection characteristics of the smaller-sized blocks. This essentially means that the pyramid arrangement of the individual microantenna blocks facilitates an efficient cascaded coupling [53] of EM energy to each individual microantenna block. In this manner, the entire micropyramid acts like an efficient broadband microresonator causing the trapped EM energy to get absorbed by the SiC material over a broad frequency range.

This effect is visualized in Fig. 4, where we depict with white streamlines the EM-energy circulation for three selected characteristic free-space wavelengths denoted as $M1$, $M2$, and $M3$. These characteristic free-space wavelengths are designated in Fig. 2(a). At the free-space wavelength denoted $M1$, which is 10.5 μm (see Fig. 2), we identify clear vortices around the sides or corners in all the SiC blocks comprising the micropyramid. These vortices in the EM-energy streamlines signify the existence of trapped cavity-type EM modes [51] in all the micropyramid's SiC blocks, similar to the ones we observe in the case of the individual blocks on their own in Fig. 3 [see Fig. 3(c) for the first block and Fig. 3(d) for the fourth block]. This means that the cavity modes in each block of the pyramid synergistically contribute toward an increased interaction between the EM field and the SiC matter in the entire pyramid that yields the strong absorption response we observe in Fig. 2(b). Indeed, the cavity-mode behavior as evidenced by the vortices in the EM streamlines leads to strongly enhanced fields within the micropyramid that we show in Fig. 4(d). For a clearer view of these fields, we also show the field values only within the micropyramid, with a saturated color map with red signifying an electric-field-intensity enhancement of 10 or larger value [see Fig. 4(g)].

On the other hand, at the free-space wavelength denoted $M3$, which is 12.0 μm, the incident EM wave essentially just streams downwards, completely avoiding the pyramid [see Fig. 4(c)]. In this case, the electric field intensity inside the micropyramid is much weaker than that of the incident light and essentially near zero for most of the micropyramid [see Figs. 4(f) and 4(i)]. As a result, the micropyramid does respond with a low reflection, albeit with little absorption, as the incident light does not interact with the SiC absorbing matter.

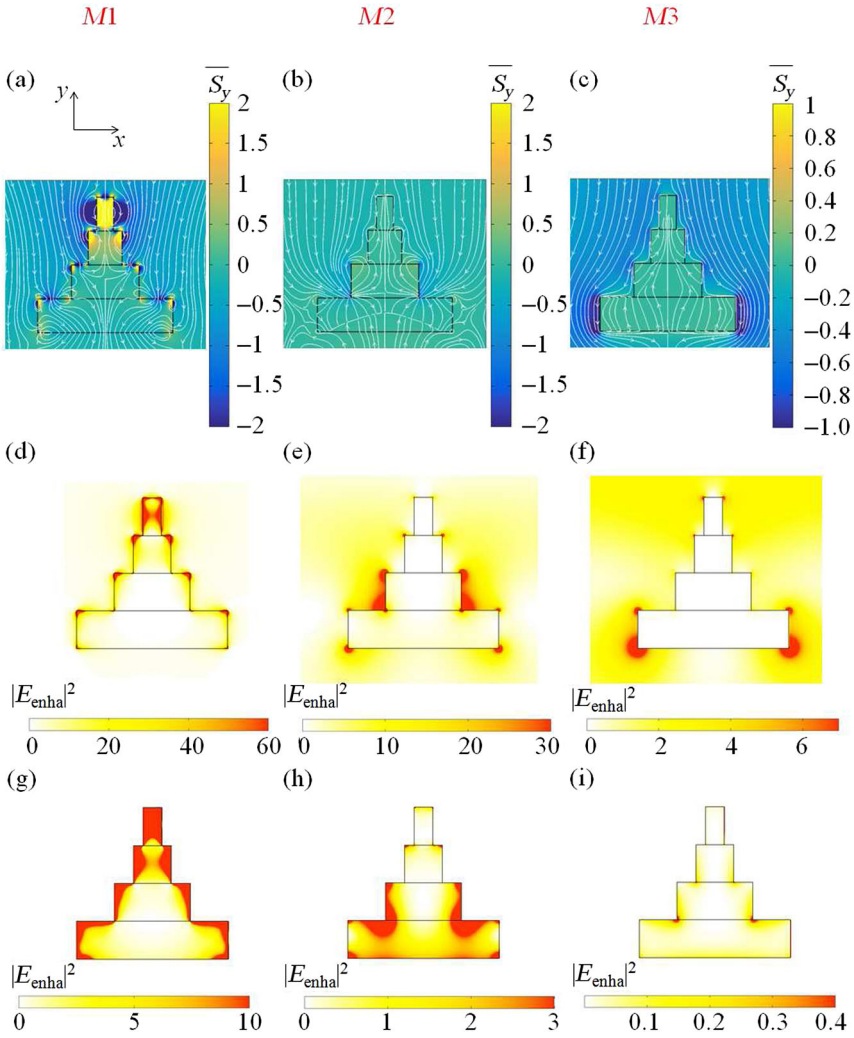

FIG. 4. (a)–(c) Energy circulation (white streamlines with arrows) around the micropyramid-array building blocks for three characteristic free-space wavelengths designated in the corresponding spectral reflectance response of Fig. 2. $M1$: Coupling to cascaded cavity resonances in the SiC blocks. $M2$: Fano interference. $M3$: EM energy streams downwards through the voids. Note, the background color map represents the y component of the time-averaged Poynting vector $\mathbf{S}$ [49]; hence, negative values represent a downward EM flow. (d)–(f) Corresponding electric-field-intensity enhancement. (g)–(i) Same as in (d)–(f) but only the electric-field-intensity enhancement inside the micropyramid is shown with a saturated color map (red is used for any electric-field-intensity enhancement that is higher than the maximum value of the associated color map).

For completeness, we also depict the situation at the free-space wavelength $M2$, which is 11.2 μm. This represents the transition from the block-cavity resonant response (for the free-space wavelengths in the spectrum around $M1$), where the micropyramid is a strong absorber, to the EM downstreaming via the voids (for the free-space wavelengths in the spectrum around $M3$), where the micropyramid is quite transparent. At this transitional regime, we neither observe strong vortices nor a downstreaming around the pyramid [see Fig. 4(b)], and the electric-field-intensity enhancement within the micropyramid is moderate [see Figs. 4(e) and 4(h)]. This situation actually represents the Fano interference [47] between the localized type of modes existing in the spectrum around $M1$ and the extended modes existing in the spectrum around $M3$ that results in the pronounced reflection peak that we observe in Fig. 2.

V. HARNESSING SUPERABSORPTION IN THE MICROPYRAMID-ARRAY SYSTEM

The focus of our discussion from here on is only within the spectral regime around free-space wavelength $M1$, where the block-cavity modes responsible for the absorption enhancement are excited. Thus far, we have discussed the broadband absorption-enhancement capabilities for sparse micropyramid arrays, with a micropyramid separation of 10 μm. This means that the cavity modes in each micropyramid interact very weakly since they are spatially apart by about a wavelength. It is, therefore, interesting to explore how the cavity modes are affected when they can interact more strongly and whether such stronger interaction can yield a stronger absorption-enhancement phenomenon.

We, therefore, calculate the spectral reflection and absorption response of arrays with closer-spaced micropyramids. We show the results in Fig. 5 for interspacings of 7.5 and 5.0 μm with dashed red and solid blue lines, respectively, along with the original micropyramid array for comparison (black dotted lines). We observe in Fig. 5(a) that the moth-eye-like SiC micropyramid building blocks continue to possess the broad-spectrum reflectionless capability, even when placed very closely. In particular, the array of micropyramid interspacings of 5.0 μm leaves only small 1-μm-wide voids at the base of the pyramid for light to squeeze through; this is about one-tenth the impinging light's wavelength. Yet, impressively, it still possesses a near-reflectionless spectral response between 10.3 and 11 μm. We attribute this to the efficient cascaded coupling to each of the microantenna cavity modes of the individual blocks.

Accordingly, since almost all impinging EM energy is injected into the micropyramid-array system in all cases, the key to the respective absorption performance lies in the electric field reconfiguration that results from the interaction between the cavity modes in the adjacent

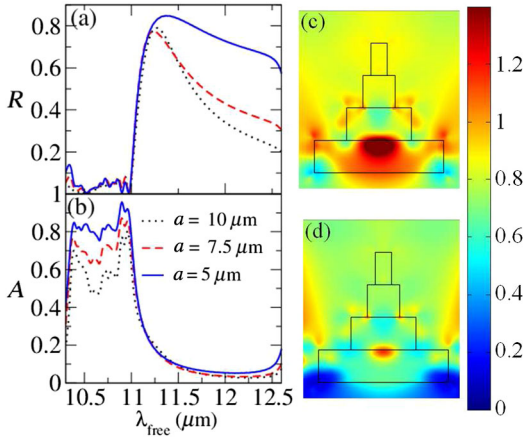

FIG. 5. (a) Spectral reflectance R for the new arrays with micropyramid interspacings $a = 7.5$ μm (dashed red lines) and $a = 5$ μm (solid blue lines). The reflectance of the original array with interspacing $a = 10$ μm (dotted black lines) is also shown for comparison. (b) Same as in (a) but for the absorptance A. (c) Electric field intensity for the array with interspacing $a = 7.5$ μm with respect to the corresponding values of the original micropyramid array with $a = 10$ μm. (d) Same as in (c) but for the array with interspacing $a = 5$ μm.

micropyramids. Since the power-dissipation rate per volume is proportional to the electric field intensity [see Eq. (A3)], we can infer that the higher the electric field intensity, the better the absorption performance. However, we should not quickly deduce from this fact that the integrated electric field intensity within the micropyramid in the new closer-spaced arrays needs to be higher in comparison with the one of the original micropyramid array. It needs only to be higher than the ratio of the micropyramid interspacing a in the newly considered arrays over the respective value of the original array. This is because, for example, an array with half the micropyramid interspacing of the original array has twice as much SiC material underneath the same illumination area in comparison to the original array. This can be clearly understood in the Appendix, where we derive an analytic expression that explicitly relates the absorption by the SiC micropyramid array with the integrated normalized electric field intensity within the SiC material and the array's micropyramid interspacing a [see Eq. (A6) in the Appendix].

In order to get a feeling for the electric field reconfiguration emanating from the strong coupling between the adjacent cavity modes, we plot the ratio between the electric field intensity in each location in the vicinity of the SiC micropyramid in the new arrays and the respective value in the original micropyramid array. The results are shown in Figs. 5(c) and 5(d) for the respective cases of micropyramid interspacings of $a = 7.5$ μm and $a = 5.0$ μm. Indeed, we observe a strong electric field reconfiguration as a result of the strong coupling between the adjacent

micropyramid modes. We observe that there are locations where the electric field intensity is even enhanced; however, in other areas, we see that electric field intensity is weakened. If we now calculate the integrated value of the normalized electric field intensity E_{norm} [48] at a free-space wavelength of 10.5 μm over the extent of the SiC micropyramid structure, for both the new arrays, we find that

$$\frac{\int |E_{\mathrm{norm}}|^2 dxdy|_{a=7.5\ \mu\mathrm{m}}}{\int |E_{\mathrm{norm}}|^2 dxdy|_{a=10\ \mu\mathrm{m}}} \sim 86.1\% \tag{2}$$

and

$$\frac{\int |E_{\mathrm{norm}}|^2 dxdy|_{a=5\ \mu\mathrm{m}}}{\int |E_{\mathrm{norm}}|^2 dxdy|_{a=10\ \mu\mathrm{m}}} \sim 68.5\%. \tag{3}$$

From Eqs. (2) and (3), we expect that at the free-space wavelength of 10.5 μm, in the new arrays with $a = 7.5$ μm and $a = 5.0$ μm, the absorption should be enhanced by respective factors of approximately 1.15 and approximately 1.35 [54] with respect to the absorption of the original array with $a = 10$ μm. The expected absorption-enhancement factors due to the electric field reconfiguration, as we quote above, are in excellent agreement with the observed absorption enhancement that we observe in Fig. 5(b).

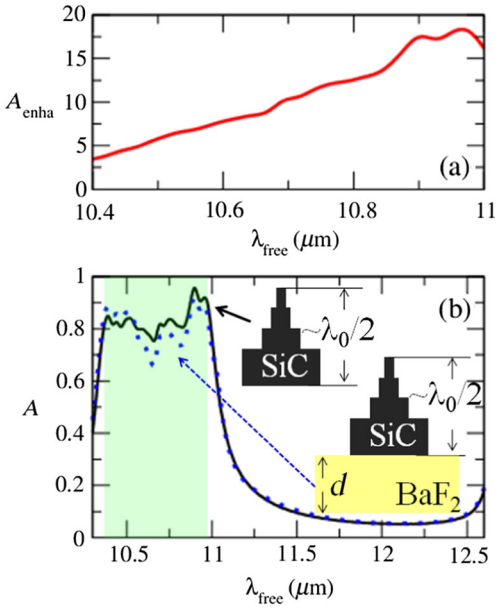

FIG. 6. (a) Absorption enhancement A_{enha} exhibited by the micropyramid-array superabsorber of interspacing $a = 5$ μm. (b) The influence of a BaF_2 substrate of thickness $d = 10$ μm on the absorptance A is shown with a dotted blue line. For comparison, the absorptance for the array without the substrate is shown with a solid black line. The green shaded area designates the spectrum where the micropyramid array with interspacing $a = 5$ μm behaves as a superabsorber [31].

VI. PERFORMANCE AND ROBUSTNESS OF THE MICROPYRAMID-ARRAY SUPERABSORBER

The closer-spaced micropyramid array with interspacing of $a = 5.0$ μm demonstrates an extraordinary—more than 80% absorptance—over a broad wavelength range between roughly 10.4 and 11 μm, thus, behaving as a superabsorber [31]. Note that such superabsorber behavior represents an extraordinary absorption enhancement in this range with respect to the absorption achieved by a bulk SiC slab that is about a wavelength thick [see Fig. 6(a)]. Such broadband superabsorber behavior is not affected by the presence of a transparent material substrate. We observe in Fig. 6(b) that the absorptance remains unaffected if the micropyramid array is placed on a 10-μm-thick BaF_2 substrate (dotted blue line in the figure). Note that BaF_2 is a fairly transparent material in the mid-IR wavelength range. For the calculations of Fig. 6(b), we take the refractive index of BaF_2 to be equal to 1.36.

Moreover, we find that the micropyramid design does not show sensitivity with respect to the alignment of the individual blocks. We show indicatively in Figs. 7(a) and 7(b) with a solid black line the results for the reflectance R and the absorptance A, respectively, for the case of a misaligned-micropyramid array. For comparison, the results for the symmetric micropyramid design are also depicted with dotted green lines. The off-center shift of the misaligned-pyramid design (see schematic in the top right panel of Fig. 7) is 150 nm for the first block, 100 nm for the second block, and 250 nm for the third block. We also show the EM-energy circulation around the misaligned micropyramid in Fig. 7(c), along with the result for the corresponding symmetric design, i.e., the design without misalignment [seen in Fig. 7(d)].

The depicted energy circulation is for wavelength $M1$ designated with the red vertical line in the figure, for which cavity-localized modes are excited in the individual blocks. We observe in Fig. 7(c) the characteristic vortexlike EM circulation along the sides or corners of the individual blocks. This EM circulation is similar to the one seen in Fig. 7(d) for the corresponding symmetric micropyramid or the modes we observe in Fig. 4(a) (for the micropyramid array with interspacing $a = 10$ μm). What is different here for the misaligned-pyramid design is that the mode field or energy landscape ceases to show the mirror symmetry with respect to the center axis of each individual block, which is the case for the x-axis symmetric pyramid designs of Figs. 4(a) and 7(d). In fact, coupling to a certain side and/or corner appears stronger than the other. However, we see that the cascaded coupling from block to block is not obstructed. Therefore, the micropyramid still shows a low-reflection or high-absorption response in the wavelength regime around $M1$ (shaded green area in the figure), as we observe in Figs. 7(a) and 7(b).

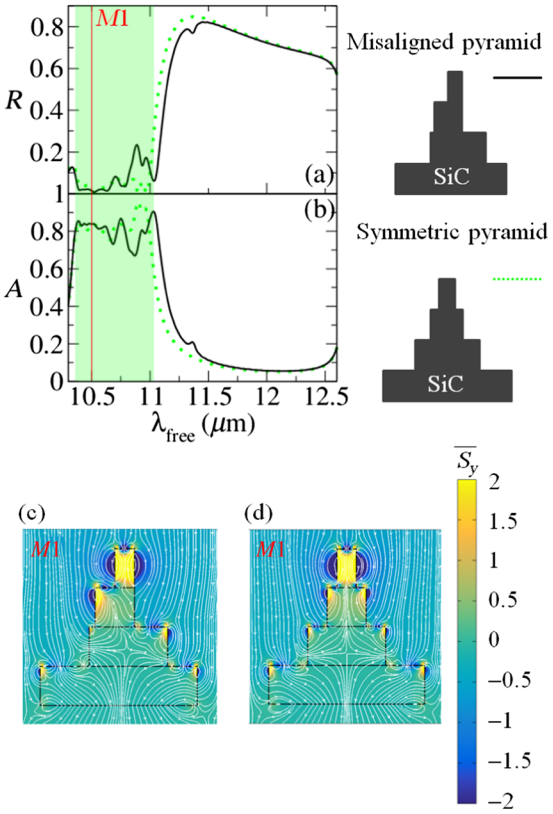

FIG. 7. Spectral response of reflectance (a) and absorptance (b). Results are shown with a solid black line for the case of a misaligned-pyramid array [see schematic depicted at the right of (a)]. The corresponding results for the symmetric micropyramid design [depicted at the right of (b)] are also shown with a dotted green line for comparison. The shaded green area represents the spectrum where localized cavity resonances are excited in the individual blocks. The corresponding EM-energy circulation for wavelength $M1$ designated with the vertical line in (a) and (b) is shown in (c) for the misaligned-pyramid array and in (d) for the corresponding symmetric one. Note that as in Figs. 4(a)–4(c), the background in (c) and (d) represents the y component of the time-averaged Poynting vector [49].

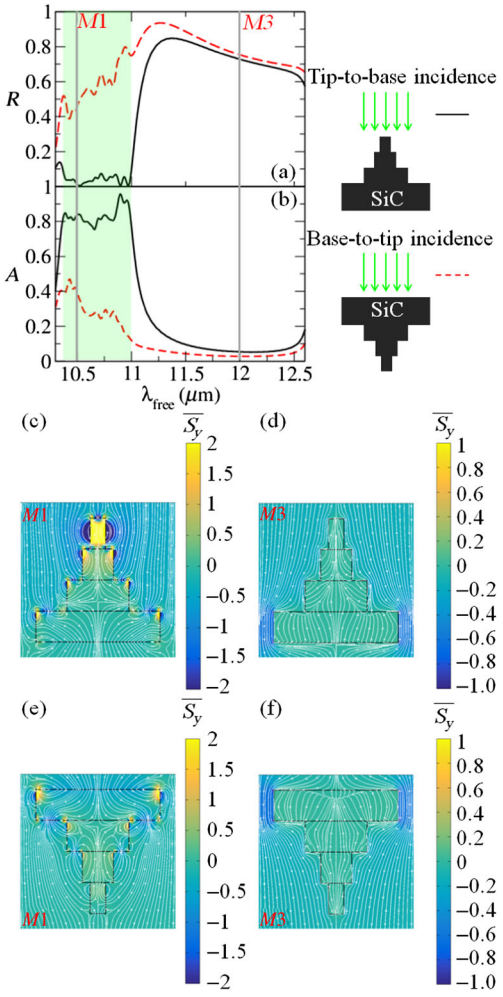

FIG. 8. Strongly asymmetric reflection or absorption response of the micropyramid-array system with $a = 5$ μm. The reflection R and absorption A for EM waves incident from the tip side of the micropyramid are shown with solid black lines in panels (a) and (b), respectively. Conversely, R and A are shown with dashed red lines in the same figures for EM waves incident from the base side of the micropyramid a. The green shaded area designates the spectral regime with a strong asymmetry in the reflection or absorption response between the tip-to-base and base-to-tip incidence. (c),(d) EM-energy circulation for wavelengths $M1$ and $M3$ for the case of incidence from the tip side of the micropyramid. (e),(f) EM-energy circulation for wavelengths $M1$ and $M3$ for the case of incidence from the base side of the micropyramid. The wavelengths $M1$ and $M3$ are designated in (a) and (b) with gray vertical lines. Note that as in Figs. 4(a)–4(c), the background in (c)–(f) represents the y component of the time-averaged Poynting vector [49].

VII. STRONGLY ASYMMETRIC RESPONSE IN THE SUPERABSORBER BEHAVIOR OF THE MICROPYRAMID ARRAY

In all the results we show thus far, light is incident from the tip side of the micropyramid. It is interesting to see what happens if we reverse the micropyramid, so light is incident from the base side toward the tip of the micropyramid. We show the results for the reflection and absorption response of the reversely oriented micropyramid in Figs. 8(a) and 8(b), respectively. It is impressive to observe that the broadband superabsorption behavior of the micropyramid strongly depends on the direction the light is coming from. In fact, we see that if we reverse the micropyramids in the array, absorption decreases dramatically [see red dashed lines in Fig. 8(b)]. In other words, the micropyramid array is only a powerful absorber for light impinging from the pyramids' tip side.

We stress that such interesting strongly asymmetric response is not a mere outcome of the y-axis-asymmetric shape of the micropyramids. For example, an identical pyramid made from a nonlossy optical material will not exhibit any asymmetric reflection response at all. In such

nonlossy structure, Lorentz reciprocity [55,56], which mandates transmission T to be symmetric, i.e., the same both for tip-to-base and base-to-tip incidence, mandates also reflection R to be symmetric. This is because in the absence of optical loss $R = 1 - T$. Now, in the lossy SiC micropyramid array, we see that reflection can be highly asymmetrical. However, this does not mean that the system becomes nonreciprocal. Indeed, the system is Lorentz reciprocal with the transmission being the same for both tip-side and base-side incidence. Now, since $R = 1 - T - A$, both reflection R and absorptance A can become highly asymmetric while transmission T is symmetric.

In other words, material optical loss is necessary to obtain any asymmetry effects in reflection or absorption. Although necessary, optical material loss by itself is not sufficient to produce strongly asymmetric effects in reflection or absorption. The highly asymmetric behavior of the micropyramid array in the reflection and absorption is a result of the coupling to the cavity modes of the block encountered by the impinging light and subsequent cascaded coupling to the cavity modes of the remaining SiC blocks [see Figs. 8(c) and 8(e)]. Note that for the same SiC micropyramid array at the frequency regime where the block-cavity modes are not excited (i.e., outside the green shaded area in Fig. 8) [see Figs. 8(d) and 8(f)], the reflection and absorption are similar for both tip-side and base-side incidence. This observation stresses that a high dielectric loss factor in an asymmetrically shaped structure does not necessarily imply a strongly asymmetric reflection or absorption response. Our results indicate that the key protagonists to an asymmetric absorption or reflection response are cascaded resonances with highly asymmetric in-coupling. This new physical insight uncovered by our work establishes a transferable design principle towards achieving a strongly asymmetric reflection or absorption in other systems.

We note in passing that asymmetric absorption or reflection effects, albeit much weaker in comparison with the ones shown in Fig. 8, have been also reported with plasmonic systems in the visible range [57–59]. Also, although not originally studied within this context, plasmonic metasurface structures that are impedance matched with vacuum connected to a ground plane via a dielectric spacer [60–62], are expected to respond with a highly asymmetric absorption or reflection. However, in this class of systems, the plasmonic absorber material is separated by a dielectric spacer with a lower thermal conductivity which may limit their functionality as thermal emitters. In contrast, our proposed SiC micropyramid design involves a single kind of connected absorber material of high thermal conductivity.

In the following section, we explore whether this observed asymmetric absorption response of the SiC micropyramid system can be further enhanced to achieve a near-unidirectional absorption or emission behavior. Our objective is to harness reflection to achieve as close as possible the following target: zero reflection for tip-to-base incidence and unity reflection for base-to-tip incidence, with transmission being zero for both incidences. It is important to have as close as possible to a zero transmission, i.e., an opaque behavior. Actually, opacity is a necessary condition to perfect emissivity as a nonzero transmission makes a medium less emissive. Note, in the extreme case of a transparent system (i.e., with transmission 1), emissivity is always zero [63]. A zero reflection for tip-to-base incidence and unity reflection for base-to-tip incidence, with opacity, implies a unity absorption for tip-to-base incidence and a zero absorption for base-to-tip incidence. Then, Kirchhoff's law states [34,35] that at a certain temperature T_{temp} and wavelength λ, the emissivity e of an opaque structure towards a certain direction equals the absorptance A for the same structure for light incident from that direction. In other words,

$$e(\lambda, T_{\text{temp}}; \text{base to tip}) = A(\lambda, T_{\text{temp}}; \text{tip to base}) = 1 - R(\lambda, T_{\text{temp}}; \text{tip to base}), \quad (4)$$

$$e(\lambda, T_{\text{temp}}; \text{tip to base}) = A(\lambda, T_{\text{temp}}; \text{base to tip}) = 1 - R(\lambda, T_{\text{temp}}; \text{base to tip}). \quad (5)$$

Equations (4) and (5) make it clear why an opaque micropyramid system, with perfectly asymmetric reflection, zero and 1, respectively, for base-to-tip and tip-to-base incidence, emits only in the direction from the base to the tip of the micropyramid. In the following, we investigate enhancing the observed asymmetry in absorption or reflection of the system of Fig. 8, as close as possible to the aforementioned perfect condition in order to enable a near-unidirectional emitter behavior for the micropyramid array.

VIII. NEAR UNIDIRECTIONAL-SUPERABSORBER AND -SUPEREMITTER BEHAVIOR OF THE MICROPYRAMID ARRAY

First, in order to strengthen the asymmetric reflection or absorption response of the micropyramid array, we explore increasing the thickness of the fourth block, while keeping the entire micropyramid thickness subwavelength (about half the free-space wavelength). Therefore, we increase the thickness of the micropyramid's base block from 1 to 3 μm and refer to this modified micropyramid-array design as design B. In this section, we focus only on the frequency regime where cavity modes are excited. As we discuss in Sec. VII, this is the frequency region with the potential for a strongly asymmetric response. The top-left panel of Fig. 9 depicts the spectral reflection response, while the bottom-left panel of Fig. 9 depicts the spectral absorption response of the design B micropyramid array. The black solid lines represent the result for tip-to-base incidence, while the red solid lines represent the result for base-to-tip incidence. The results of the original design of Fig. 8,

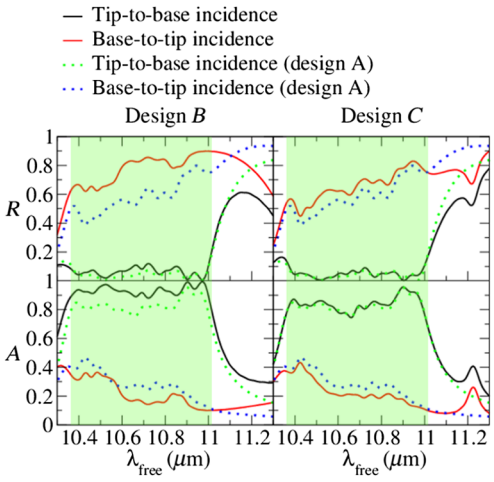

FIG. 9. Enhancing the asymmetry in the reflection or absorption response between tip-to-base and base-to-tip incidence by considering a thicker 3-μm-thick block for the pyramid base (design B) or by bringing the micropyramids closer at an interspacing of 4.2 μm (design C). The reflectance R (top panels) and absorptance A (bottom panels) are shown for each design with black solid lines (red solid lines) for tip-to-base (base-to-tip) incidence. For comparison, the respective results for the design of Fig. 8 (design A) are shown with green dotted lines (tip-to-base incidence) and blue dotted lines (base-to-tip incidence). The green shading designates the frequency region of strong asymmetry in the reflection or absorption response between tip-to-base incidence and base-to-tip incidence.

which we refer to as design A from hereon, are also included in Fig. 9 for comparison. The green dotted lines designate the response of the original design A array for tip-to-base incidence, while the blue dotted lines designate the corresponding response for base-to-tip incidence.

We observe an increased reflection for the base-to-tip incidence for the modified design B array which results in a reduced absorption when compared with the original design A array. We attribute this increased reflection to the larger size of the SiC block which comes at first contact with the impinging light for the base-to-tip incidence case. At the same time, for tip-to-base incidence, we do not see any significant changes in the reflection response. This is because for such case, the first three blocks that the incident EM encounters are identical with the original design A array. However, the absorption ends up being larger in the modified design B array for tip-to-base incidence. This is because the same EM energy that gets sequentially coupled to the last block now interacts with a larger volume of lossy matter. The combined effect of absorption decrease for base-to-tip incidence with absorption increase for tip-to-base incidence leads to a stronger asymmetry in the absorption response.

Second, we explore the effect of bringing the micropyramids closer. Therefore, we start from the original design, design A, and bring each micropyramid building block closer at an interspacing of 4.2 μm. We refer to this modified design as design C. We show the results for the reflection and absorption response in the top-right and bottom-right panels of Fig. 9, respectively. Here also, the black solid lines designate the results for tip-to-base incidence, while the red solid lines designate the results for base-to-tip incidence. Like in the cases of the left panels of Fig. 9, the original design A results are depicted as well for comparison purposes. Indeed, as expected, this closer-spaced array shows a larger reflection and so a smaller absorption for base-to-tip incidence. This is because, for such case, the wave encounters thick closely spaced SiC blocks resulting in a weaker coupling to the cavity modes. On the other hand, the tip-to-base incidence case is not affected much by bringing the micropyramids closer, as the wave still first encounters relatively sparsely spaced small SiC blocks. Accordingly, since absorption does not change for tip-to-base incidence but decreases for base-to-tip incidence when compared with the original design A array, the net effect is that the asymmetry in the absorption response becomes stronger for the modified design C microarray.

We then explore if both effects of asymmetry enhancement in the response of the two aforementioned designs can

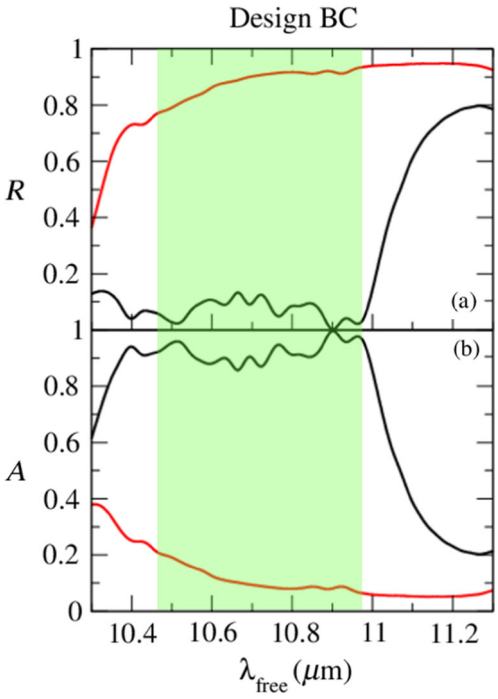

FIG. 10. The micropyramid as a near-unidirectional absorber or emitter. Reflection R (a) and absorption A (b) versus the free-space wavelength are shown for a micropyramid-array design (design BC) with interspacing $a = 4.2$ μm and micropyramid block sizes same as the design of Figs. 2 and 4 except for the fourth block being thicker (3 μm thick). The green shading designates a frequency regime where the micropyramid absorbs with near 100% efficiency when light is incident from the tip side of the micropyramid, while it absorbs weakly less than 20% when light is incident from the base side of the micropyramid in this manner acting as a near-unidirectional absorber or emitter.

work in synergy when combined into one micropyramid-array design. We, therefore, explore a design where the micropyramids are more closely spaced at 4.2 μm and have also their base block thicker (3 μm versus 1 μm of the original design of Fig. 8) (design BC). We show the results for design BC in Fig. 10(a) for the reflection response and Fig. 10(b) for the absorption response. Black solid and red solid lines represent the results for tip-to-base and base-to-tip incidence, respectively. Indeed, we find that the asymmetry in the absorption response gets further enhanced.

In particular, in the frequency region represented with the green shading in Fig. 10, we observe that the absorption is near unity for tip-to-base incidence and very small (less than 20%) for base-to-tip incidence. Essentially, the micropyramid array is an effective absorber only for light incident from the tip side of the micropyramid. Moreover, in the green shaded region, the micropyramid system is near opaque with transmission less than 2%. Accordingly, Eqs. (4) and (5) suggest that the micropyramid system of Fig. 10 emits predominantly only in the direction from the micropyramid's base towards the tip. To be specific, the emission in the base-to-tip direction is in the range of 5 to 15 times stronger in the wavelength spectrum designated with the green shaded area in Fig. 10 with respect to the emission in the tip-to-base direction. In other words, the micropyramid array of Fig. 10 behaves as a near-unidirectional absorber or emitter.

IX. CONCLUSIONS

We present a stepped micropyramid SiC array structure with superabsorber capabilities over a broad spectral range within the SiC phonon-polariton gap (reststrahlen band). For TH-polarized light, this structure acts simultaneously as a moth-eye antireflector, allowing almost all light to couple inside, and as a broadband microantenna. The superabsorber capabilities emanate from the cascaded coupling of the corner- or side-vortex modes at each of the SiC blocks comprising the micropyramid. The cascaded coupling of such modes from block to block of the lossy SiC micropyramid system along with the asymmetric in-coupling to these modes are the key protagonists that enable a highly unidirectional reflection or absorption response. Specifically, the micropyramid system is a strong absorber only for light impinging from the tips to the bases of the micropyramids. These results and physical insight for the underpinning mechanisms provide transferable design principles towards achieving a strongly asymmetric broadband reflection or absorption in other systems. Furthermore, we discuss how the SiC micropyramid system, when near opaque with a highly asymmetric reflection or absorption, behaves as a near-unidirectional emitter by virtue of Kirchhoff's law [34,35].

Our proposed platform can be applied in improving the efficiency and directionality of infrared globar-type sources [64]. Moreover, the operational bandwidth of this system falls within the atmospheric transparency window [28,29]. At the same time, SiC is a weakly absorbing material for most of the solar radiation spectrum. These two facts in combination suggest that the micropyramid-array platform can be highly relevant to the emerging area of passive radiative cooling, a promising avenue for cooling buildings and vehicles [27,65]. The highly unidirectional emission characteristics of our proposed platform may inspire designs for temperature management of electronic and plasmonic devices [66,67], which is crucial to their resilience and functionality. Moreover, our system studied here may inspire structures comprising other infrared active materials that can improve the sensitivity of infrared cameras and detectors [6].

ACKNOWLEDGMENTS

Financial support for the Ph.D. studentship of G. C. R. Devarapu by the College of Engineering, Mathematics and Physical Sciences, University of Exeter is acknowledged.

APPENDIX: ABSORPTANCE AND ELECTRIC FIELD INTENSITY IN THE MICROPYRAMID ARRAY

In the following, we derive an expression yielding the absorptance through the micropyramid array A versus the electric field intensity within the bounds of the micropyramid building block in each unit cell of the array. The total absorption through the stepped micropyramid array should be the sum of the respective absorption $A(i)$ provided by each of the constituent blocks of the SiC pyramid structure, i.e.,

$$A = \sum_{i=1}^{4} A(i). \tag{A1}$$

The fraction of incident power that gets absorbed within the ith SiC building block of the micropyramid $A(i)$ can be obtained as

$$A(i) = \frac{\overline{P_{\mathrm{loss},i}}}{\overline{P_{\mathrm{inc}}}}, \tag{A2}$$

where $\overline{P_{\mathrm{loss},i}}$ represents the time-averaged power dissipation in the ith SiC building block in the elementary unit cell of the micropyramid array. Conversely, $\overline{P_{\mathrm{inc}}}$ represents the time-averaged power incident on the elementary unit cell of the micropyramid array. As there is translational symmetry along the z direction, we consider the EM power that impinges through an area of $A_{\mathrm{inc}} = a l_z$, with l_z being the length of an arbitrary segment along the z direction of the SiC block and a being the micropyramid's interspacing (see Fig. 11).

From Poynting's theorem [68], we have that the time-averaged power dissipation per unit volume of a material $\overline{P_{\mathrm{loss},v}}$ is given by

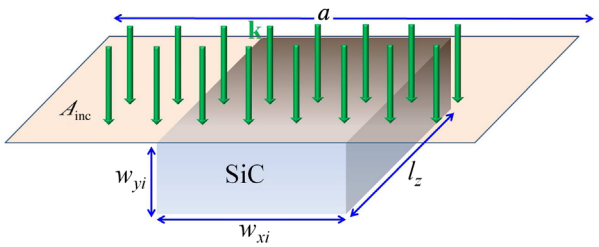

FIG. 11. EM radiation impinging onto the ith SiC block of the micropyramid in the elementary unit cell of the array with periodicity a. The widths in the x and y directions of the block are designated. Because of translation symmetry in the z direction, the segment with length l_z is chosen arbitrarily.

$$\overline{P_{\text{loss},v}} = \frac{\omega\varepsilon_0\varepsilon_r''(\omega)}{2}|E|^2, \tag{A3}$$

where ε_0 is the vacuum permittivity and $\varepsilon_r''(\omega)$ the imaginary part of the relative permittivity of the material at the frequency ω of the impinging wave. Therefore, the power dissipated within the volume $V_i = w_{xi}w_{yi}l_z$ in the ith SiC micropyramid block in the elementary unit cell in the array $\overline{P_{\text{loss},i}}$ is

$$\overline{P_{\text{loss},i}} = \frac{\omega\varepsilon_0\varepsilon_r'' l_z}{2}\int_0^{w_{xi}}\int_0^{w_{yi}}|E(x,y)|^2 dxdy, \tag{A4}$$

where the widths w_{xi}, w_{yi} are depicted in the schematics of Fig. 11. Note that in the above integration, the (x, y) Cartesian coordinates are offset to be zero at the bottom left corner of the ith SiC block in the micropyramid.

On the other hand, the time-averaged incident power $\overline{P_{\text{inc}}}$ through the area A_{inc} depicted in the schematics of Fig. 11 is

$$\overline{P_{\text{inc}}} = \frac{al_z}{2c\mu_0}|E_{\text{inc}}|^2, \tag{A5}$$

where μ_0 is the vacuum permeability and c the vacuum speed of light. Now if we input the expressions of Eqs. (A4) and (A5) into Eq. (A2) we obtain

$$\begin{aligned} A(i) &= \frac{\varepsilon_r''(\omega)\varepsilon_0\mu_0\omega c}{a|E_{\text{inc}}|^2}\int_0^{w_{xi}}\int_0^{w_{yi}}|E(x,y)|^2 dxdy \\ &= \frac{\varepsilon_r''\omega}{ac}\int_0^{w_{xi}}\int_0^{w_{yi}}|E_{\text{norm}}(x,y)|^2 dxdy, \end{aligned} \tag{A6}$$

where $|E_{\text{norm}}(x,y)| = [|E(x,y)|/|E_{\text{inc}}|]$ represents the magnitude of the electric field within the SiC block normalized by the magnitude of the incident electric field occurring when an incident wave of frequency ω is incident on the structure. In other words, $|E_{\text{norm}}(x,y)|$ represents the electric field enhancement at a certain location (x, y) within the ith SiC block of the micropyramid. Equation (A6) underlines the importance of obtaining an enhanced electric field in areas within the micropyramid (as we see in Fig. 4) in order to obtain an enhanced absorption. This fact, in turn, stresses the key role of the block-cavity modes in obtaining a strong absorption response. The total absorption through the entire micropyramid can be then obtained from the summation of the respective absorptions $A(i)$ in each of the SiC blocks.

[1] H. A. Atwater and A. Polman, Plasmonics for improved photovoltaic devices, Nat. Mater. **9**, 205 (2010).

[2] K. Aydin, V. E. Ferry, R. M. Briggs, and H. A. Atwater, Broadband, polarization-independent resonant light absorption using ultrathin, plasmonic super absorbers, Nat. Commun. **2**, 517 (2011).

[3] R. A. Pala, J. White, E. Barnard, J. Liu, and M. L. Brongersma, Design of plasmonic thin film solar cells with broadband absorption enhancements, Adv. Mater. **21**, 3504 (2009).

[4] C. Lin and M. L. Povinelli, Optical absorption enhancement in silicon nanowire arrays with a large lattice constant for photovoltaic applications, Opt. Express **17**, 19371 (2009).

[5] C. M. Watts, X. Liu, and W. J. Padilla, Metamaterial electromagnetic wave absorbers, Adv. Mater. **24**, OP98 (2012).

[6] A. V. Barve, S. J. Lee, S. K. Noh, and S. Krishna, Review of current progress in quantum dot infrared photodetectors, Laser Photonics Rev. **4**, 738 (2010).

[7] J. A. Mason, S. Smith, and D. Wasserman, Strong absorption and selective thermal emission from a midinfrared metamaterial, Appl. Phys. Lett. **98**, 241105 (2011).

[8] Y. D. Sharma, Y. C. Jun, J. O. Kim, I. Brener, and S. Krishna, Polarization-dependent photocurrent enhancement in metamaterial-coupled quantum dots-in-a-well infrared detector, Opt. Commun. **312**, 31 (2014).

[9] M. A. Kats, D. Sharma, J. Lin, P. Genevet, R. Blanchard, Z. Yang, M. M. Qazilbash, D. N. Basov, S. Ramanathan, and F. Capasso, Ultra-thin perfect absorber employing a tunable phase change material, Appl. Phys. Lett. **101**, 221101 (2012).

[10] D. Shrekenhamer, J. Montoya, S. Krishna, and W. J. Padilla, Four-color metamaterial absorber THz spatial light modulator, Adv. Opt. Mater. **1**, 905 (2013).

[11] W. Streyer, S. Law, A. Rosenberg, C. Roberts, V. A. Podolskiy, A. J. Hoffman, and D. Wasserman, Engineering absorption and blackbody radiation in the far-infrared with surface phonon polaritons on gallium phosphide, Appl. Phys. Lett. **104**, 131105 (2014).

[12] B. Neuner III, C. Wu, G. T. Eyck, M. Sinclair, I. Brener, and G. Shvets, Efficient infrared thermal emitters based on low-albedo polaritonic meta-surfaces, Appl. Phys. Lett. **102**, 211111 (2013).

[13] A. Vora, J. Gwamuri, J. M. Pearce, P. L. Bergstrom, and D. O. Guney, Multi-resonant silver nano-disk patterned thin film hydrogenated amorphous silicon solar cells for Staebler-Wronski effect compensation, J. Appl. Phys. **116**, 093103 (2014).

[14] W. Cai and V. Shalaev, *Optical Metamaterials Fundamentals and Applications* (Springer, New York, 2010).

[15] C. M. Soukoulis and M. Wegener, Past achievements and future challenges in the development of three-dimensional photonic metamaterials, Nat. Photonics **5**, 523 (2011).
[16] N. I. Landy, S. Sajuyigbe, J. J. Mock, D. R. Smith, and W. J. Padilla, Perfect Metamaterial Absorber, Phys. Rev. Lett. **100**, 207402 (2008).
[17] A. Balmakou, M. Podalov, S. Khakhomov, D. Stavenga, and I. Semchenko, Ground-plane-less bidirectional terahertz absorber based on omega resonators, Opt. Lett. **40**, 2084 (2015).
[18] J. J. Liu, G. V. Naik, S. Ishi, C. DeVault, A. Boltasseva, V. M. Shalaev, and E. Narimanov, Optical absorption of hyperbolic metamaterial with stochastic surfaces, Opt. Express **22**, 8893 (2014).
[19] M. A. Kats, R. Blanchard, P. Genevet, and F. Capasso, Nanometre optical coatings based on strong interference effects in highly absorbing media, Nat. Mater. **12**, 20 (2013).
[20] G. C. R. Devarapu and S. Foteinopoulou, Mid-IR near-perfect absorption with a SiC photonic crystal with angle-controlled polarization selectivity, Opt. Express **20**, 13040 (2012).
[21] G. C. R. Devarapu and S. Foteinopoulou, Compact photonic-crystal superabsorbers from strongly absorbing media, J. Appl. Phys. **114**, 033504 (2013).
[22] J. L. Gray, in *Handbook of Photovoltaic Science and Engineering*, edited by A. Luque and S. Hegedus (Wiley, New York, 2010).
[23] B. Curtin, R. Biswas, and V. Dalal, Photonic crystal based back reflectors for light management and enhanced absorption in amorphous silicon solar cells, Appl. Phys. Lett. **95**, 231102 (2009).
[24] B. Lee, Il-Min Lee, S. Kima, D.-H. Oh, and L. Hesselink, Review on subwavelength confinement of light with plasmonics, J. Mod. Opt. **57**, 1479 (2010).
[25] P. B. Catrysse and S. Fan, Near-complete transmission through subwavelength hole arrays in phonon-polaritonic thin films, Phys. Rev. B **75**, 075422 (2007).
[26] A. Ganjoo, H. Jain, C. Yu, J. Irudayaraj, and C. G. Pantano, Detection and fingerprinting of pathogens: Mid-IR biosensor using amorphous chalcogenide films, J. Non-Cryst. Solids **354**, 2757 (2008).
[27] A. P. Raman, M. A. Anoma, L. Zhu, E. Rephaeli, and S. Fan, Passive radiative cooling below ambient air temperature under direct sunlight, Nature (London) **515**, 540 (2014).
[28] C. Kuenzer and S. Dech, in *Thermal Infrared Remote Sensing: Sensors, Methods and Applications*, edited by C. Kuenzer and S. Dech (Springer, New York, 2013).
[29] M. Cucumo, A. De Rosa, and V. Marinelli, Experimental testing of correlations to calculate the atmospheric transparency window emissivity coefficient, Solar Energy **80**, 1031 (2006).
[30] U. Guler, A. Boltasseva, and V. M. Shalaev, Refractory plasmonics, Science **344**, 263 (2014).
[31] With the term superabsorber, we imply a system demonstrating a strong absorption that can reach more than 80%, which at the same time represents a strong absorption enhancement with respect to the absorption exhibited by the lossy constituent material, SiC in our case, when in bulk form. Please see also references to superabsorber behavior exhibited in other systems [2,32,33].
[32] N. Zhang, K. Liu, H. Song, Z. Liu, D. Ji, X. Zeng, S. Jiang, and Q. Gan, Refractive index engineering of metal-dielectric nanocomposite thin films for optical super absorber, Appl. Phys. Lett. **104**, 203112 (2014).
[33] V. Yannopapas and I. E. Psarobas, Ordered arrays of metal nanostrings as broadband super absorbers, J. Phys. Chem. C **116**, 15599 (2012).
[34] F. E. Nicodemus, Directional reflectance and emissivity of an opaque surface, Appl. Opt. **4**, 767 (1965).
[35] Eugene A. Sharkov, *Passive Microwave Sensing of the Earth* (Springer, New York, 2003).
[36] G. C. R. Devarapu and S. Foteinopoulou, Broadband mid-IR superabsorption with aperiodic polaritonic photonic crystals, J. Eur. Opt. Soc. Rapid Publ. **9**, 14012 (2014).
[37] S. J. Wilson and M. C. Hutley, The optical properties of moth-eye, antireflection surfaces, Opt. Acta **29**, 993 (1982).
[38] P. Kunze and K. Hausen, Inhomogeneous refractive index in the crystalline cone of a moth eye, Nature (London) **231**, 392 (1971).
[39] S. L. Diedenhofen, G. Vecchi, R. E. Alga, A. Hartsuiker, O. L. Muskens, G. Immink, E. P. A. M. Bakkers, W. L. Vos, and J. G. Rivas, Broad-band and omnidirectional antireflection coatings based on semiconductor nanorods, Adv. Mater. **21**, 973 (2009).
[40] W.-L. Min, B. Jiang, and P. Jiang, Bioinspired self cleaning antireflection coatings, Adv. Mater. **20**, 3914 (2008).
[41] P. R. Villeneuve and M. Piche, Photonic bandgaps in periodic dielectric structures, Prog. Quantum Electron. **18**, 153 (1994).
[42] G. N. Yushin, A. V. Kvit, R. Collazo, and Z. Sitar, SiC to SiC wafer bonding, MRS Proc. **742** (2002).
[43] G. Subramania and S. Y. Lin, Fabrication of three-dimensional photonic crystal with alignment based on electron beam lithography, Appl. Phys. Lett. **85**, 5037 (2004).
[44] J. Y. Lee, X. Lu, and Q. Lin, High-Q silicon carbide photonic-crystal cavities, Appl. Phys. Lett. **106**, 041106 (2015).
[45] J. A. Schuller, T. Taubner, and M. L. Brongersma, Optical antenna thermal emitters, Nat. Photonics **3**, 658 (2009).
[46] Lumerical FDTD Solutions, Reference Guide for FDTD Solutions, http://www.lumerical.com/tcad-products/fdtd/.
[47] A. E. Miroshnichenko, S. Flach, and Y. S. Kivshar, Fano resonances in nanoscale structures, Rev. Mod. Phys. **82**, 2257 (2010).
[48] The electric field intensity is normalized by the electric field intensity of the impinging EM wave, $|E_0|^2$.
[49] $\bar{S_y} = -\frac{1}{2}\mathrm{Re}(E_x H_z*)$ is represented in units of $S_0 = [1/(c\mu_0)]|E_0|^2$ with $|E_0|$ being the electric field amplitude of the source.
[50] K. Feng, W. Streyer, Y. Zhong, A. J. Hoffman, and D. Wasserman, Photonic materials, structures and devices for Reststrahlen optics, Opt. Express **23**, A1418 (2015).
[51] Y.-L. Ho, L.-C. Huang, E. Lebrasseur, Y. Mita, and J.-J. Delaunay, Independent light-trapping cavity for ultrasensitive plasmonic sensing, Appl. Phys. Lett. **105**, 061112 (2014).
[52] G. Subramania, S. Foteinopoulou, and I. Brener, Nonresonant Broadband Funneling of Light via Ultrasubwavelength Channels, Phys. Rev. Lett. **107**, 163902 (2011).

[53] R. Garg and K. Thyagarajan, Cascaded coupling: Realization and application to spectral maneuvering, Opt. Fiber Technol. **19**, 148 (2013).

[54] To obtain the absorption-enhancement factors, we divide the values of Eqs. (2) and (3) with the respective ratios of the micropyramid interspacing, a.

[55] H. A. Lorentz, The theorem of Poynting concerning the energy in the electromagnetic field and two general propositions concerning the propagation of light, Versl. Kon. Akad. Wentensch. Amsterdam **4**, 176 (1896).

[56] M. Nieto-Vesperinas, *Scattering and Diffraction in Physical Optics* (Wiley, New York, 1991).

[57] E. Altewischer, M. P. van Exter, and J. P. Woerdman, Nonreciprocal reflection of a subwavelength hole array, Opt. Lett. **28**, 1906 (2003).

[58] S. Butun and K. Aydin, Asymmetric light absorption and reflection in freestanding nanostructured metallic membranes, ACS Photonics **2**, 1652 (2015).

[59] Note, the authors in Ref. [57] use the term "nonreciprocal" in the context of asymmetric reflection without violation of the Lorentz reciprocity principle.

[60] Xianliang Liu, Tatiana Starr, Anthony F. Starr, and Willie J. Padilla, Infrared Spatial and Frequency Selective Metamaterial with Near-Unity Absorbance, Phys. Rev. Lett. **104**, 207403 (2010).

[61] C. Wu and G. Shvets, Design of metamaterial surfaces with broadband absorbance, Opt. Lett. **37**, 308 (2012).

[62] A. Vora, J. Gwamuri, N. Pala, A. Kulkarni, J. M. Pearce, and D. O. Guney, Exchanging Ohmic losses in metamaterial absorbers with useful optical absorption for photovoltaics, Sci. Rep. **4**, 4901 (2014).

[63] *Theory and Practice of Radiation Thermometry*, edited by D. P. DeWitt and F. P. Incroprera (Wiley Interscience, New York, 1988), Chap 1.

[64] J. E. Stewart and J. C. Richmond, Infrared emission spectrum of silicon carbide heating elements, J. Res. Natl. Bur. Stand. **59**, 405 (1957).

[65] E. Raphaelli, A. Raman, and S. H. Fan, Ultrabroadband photonic structures to achieve high-performance daytime radiative cooling, Nano Lett. **13**, 1457 (2013).

[66] S. V. Boriskina, J. K. Tong, W.-C. Hsu, L. Weinstein, X. Huang, J. Loomis, Y. Xu, and G. Chen, Hybrid optical-thermal devices and materials for light manipulation and radiative cooling, Proc. SPIE Int. Soc. Opt. Eng. **9546**, 95461U (2015).

[67] S. V. Boriskina, J. K. Tong, W.-C. Hsu, B. Liao, Y. Huang, V. Chiloyan, and G. Chen, Heat meets light on the nanoscale, Nanophotonics **5**, 134 (2016).

[68] J. D. Jackson, *Classical Electrodynamics*, 3rd ed. (John Wiley and Sons, Hoboken, NJ, 1998).